Solar Phys (2009) 256: 41–55
DOI 10.1007/s11207-009-9355-4

Three-Dimensional Reconstruction of Active Regions

L. Rodriguez · A.N. Zhukov · S. Gissot · M. Mierla

Received: 8 December 2008 / Accepted: 1 April 2009 / Published online: 21 April 2009

Abstract The STEREO mission provides an unprecedented opportunity to reconstruct the 3D configuration of solar features. In this work, we combine SECCHI/EUVI data from both spacecraft by means of a local correlation tracking method. The technique allows an automatic (without user intervention) matching of pixels in both images. This information is then used to triangulate the 3D coordinates of each pixel. We use the method in order to reconstruct and analyze the 3D structure of active regions. In particular, we focus on the extraction of coronal loop heights, observed nearly simultaneously in the 171, 195 and 284 Å passbands. We compare the properties of loops in the different wavelengths and extract valuable information regarding their geometry. In particular, we demonstrate that some loops that look co-spatial in the 171 Å and 195 Å images have in fact different heights and thus occupy different volumes. Our results have important implications for multi-wavelength studies of coronal loops, especially for calculations using filter-ratio techniques.

1. Introduction

The twin STEREO spacecraft (Solar TErrestrial RElations Observatory, see Kaiser *et al.*, 2008) provide for the first time the opportunity to apply stereoscopy to solar images taken at the same time from different viewpoints. This information is of a vital importance in solar physics. Up to now, knowledge on the heights of features above the solar surface and on

STEREO Science Results at Solar Minimum
Guest Editors: Eric R. Christian, Michael L. Kaiser, Therese A. Kucera, O.C. St. Cyr.

L. Rodriguez (✉) · A.N. Zhukov · S. Gissot · M. Mierla
Solar-Terrestrial Center of Excellence – SIDC, Royal Observatory of Belgium, Avenue Circulaire 3, 1180 Brussels, Belgium
e-mail: rodriguez@oma.be

A.N. Zhukov
Skobeltsyn Institute of Nuclear Physics, Moscow State University, 119992 Moscow, Russia

M. Mierla
Astronomical Institute of the Romanian Academy, Str. Cutitul de Argint 5, 040557 Bucharest, Romania

speeds of dynamic events was only obtained from measurements performed in the plane of the sky, or otherwise affected by projection effects. The importance of an exact calculation of loop geometries has been underlined in the past years. For example, Alexander and Katsev (1996) raised the importance of considering the orientation of loops with respect to the line-of-sight (LOS) direction. Dymova and Ruderman (2006) found that the loop geometry has a strong influence on the calculation of the atmospheric scale height from observations of loop oscillations.

Earlier work on solar stereoscopy done before the STEREO era was carried out by assuming temporal stability of the features under study and allowing the Sun to rotate in order to have more than one viewpoint (Berton and Sakurai, 1985; Kouchmy and Molodensky, 1992; Aschwanden and Bastian, 1994; Aschwanden *et al.* 1995, 1999; Feng *et al.*, 2007a). Now, with the routine collection of the STEREO data, two viewpoints are available simultaneously thereby reducing the stereoscopic problem to the identifying and matching of the same points in the corresponding pair of images (associated with an eventual 3D reconstruction).

We, however, note that every pixel in an image is a result of the LOS integration of emission of the optically thin coronal plasma. This problem of the LOS integration remains present in the analysis of the STEREO data (there are two different lines of sight), making the matching of structures between the two images more complicated (*e.g.* Inhester, 2006). The problem is more serious for large separation angles, when the LOS differs substantially from one spacecraft to the other, and for coronal structures significantly extended along the line of sight (*e.g.* streamer belt and coronal mass ejections). Therefore, for this work we have selected periods in which the angular separation between STEREO-A and STEREO-B is small and concentrated on the analysis of coronal loops (see Section 3). The loop dimension along the LOS is most probably similar to their plane of the sky width (nearly circular cross-section), and we do not consider the question of the loop internal structure here.

There are several possible approaches for solving the identification and matching problem (see Trucco and Verri, 1998 for a general description). In particular using STEREO data, Feng *et al.* (2007b) used a loop segmentation program to extract loops from individual images that were then compared with the results of a magnetic field extrapolation model in order to match the corresponding loops in the pair of simultaneous images taken by the Extreme Ultraviolet Imager telescope, which is a part of the SECCHI instrument suite (Sun Earth Connection Coronal and Heliospheric Investigation, see Howard *et al.*, 2008 for the instrument description). Aschwanden *et al.* (2008) used a manual selection method to choose points along loops in both EUVI images, from which a curve was then interpolated. Using SECCHI/COR1 data, Mierla *et al.* (2008) manually selected points within coronal mass ejections (CMEs) in order to estimate their propagation direction and true (unprojected) speed. Patsourakos *et al.* (2008) analysed the initiation of polar coronal jets seen in SECCHI/EUVI data, also using manual selection of points. A fully automated optical flow algorithm was presented by Gissot *et al.* (2008) in order to match points in 304 Å EUVI images, with a goal to reconstruct the 3D morphology of an erupting filament.

In this work we use an automated local correlation tracking method (LCT, described in Section 2) in order to match the pixels from pairs of SECCHI/EUVI images. In Section 3, results of the method applied to active regions and coronal loops will be shown and conclusions will be then drawn in Section 4.

2. Data and Method

Three corrections need to be applied to the EUVI images prior to the analysis: the size of the solar disc, its center and its orientation need to be the same in both images. This is due to the fact that the STEREO A (Ahead) spacecraft is closer to the Sun than the STEREO B (Behind), with both spacecraft slightly out of the ecliptic plane and having different roll angles. After applying standard calibration procedures and pre-processing the images using the SolarSoft routine scc_stereopair.pro, the solar disc in the image pair has a common center and size, and the images are aligned to the STEREO mission plane (defined by the two spacecraft and the center of the Sun). This is a pre-requisite for applying stereoscopy, since the exact location of pixels in the image pair is of a vital importance.

For the analysis of images, we make use of epipolar geometry (Inhester, 2006). In this representation, epipolar planes are defined by the position of the two spacecraft and a point in the field-of-view. When these planes are projected into the 2D space of the images, they are seen as epipolar lines. A point contained in one of these lines in one image will appear on the same epipolar line on the second image. This constraint reduces greatly the problem of finding the corresponding points in both images. In particular, when epipolar lines are horizontal, then one needs to search only in one dimension in order to find the matching pixels. Nevertheless, this is not normally the case and the images need to be treated in order to obtain horizontal epipolar lines. For the case of SECCHI/EUVI images, and after the corrections described in the previous paragraph have been applied, the lines can be considered to be horizontal, and parallel to the STEREO mission plane. Since this is an epipolar plane, the result is that the epipolar north (and not the solar north) is aligned with the image north.

After the pre-processing, we apply a local correlation tracking technique (LCT, November and Simon, 1988; Trucco and Verri, 1998) in order to match automatically the points between the images. The procedure automatically selects pixels in the image taken by the A spacecraft (one by one) and searches for the best location that the corresponding pixel may have in the image taken by the spacecraft B. It uses a moving search window in which the normalized correlation is calculated, in the following way:

$$\sigma_{\mathrm{AB}}(x, y) = \frac{\sum I_{\mathrm{A}}(x, y) I_{\mathrm{B}}(x + \Delta X, y + \Delta Y)}{[\sum I_{\mathrm{A}}^2(x, y) \sum I_{\mathrm{B}}^2(x + \Delta X, y + \Delta Y)]^{1/2}}, \tag{1}$$

where σ_{AB} represents the correlation value, I_{A} and I_{B} are the brightness in the corresponding pixels from images EUVI-A and EUVI-B, ΔX and ΔY are the shifts inside the window where the correlation is taking place. The location of the pixel in the image B at which the correlation is maximized is then selected as the matching location for the corresponding pixel in the image A. Since, as stated before, the points in one image are located along the same epipolar line on the second image, the difference in the location of a point between the two images can be expressed as a horizontal displacement. Once this information is known, together with the geometry of the system, the 3D coordinates of the point can be calculated. We use here the same geometry and assumptions as Gissot *et al.* (2008), with the final reconstruction formula given by:

$$R^2 = X_{\mathrm{A}}^2 + Y_{\mathrm{A}}^2 + \left[\tan\left(\frac{\Delta\lambda}{2}\right) X_{\mathrm{A}} + \frac{\Delta X}{\sin \Delta\lambda}\right]^2, \tag{2}$$

here R is the (3D) distance of the point from the Sun's center, X and Y are the coordinates of the pixel in the image A, $\Delta\lambda$ is the angular separation between the two spacecraft and ΔX is the displacement of the point between the two images as obtained from the LCT method.

The procedure is repeated automatically for every pixel in the EUVI-A image. The application of the procedure to the on-disc pixels close to the solar limb may lead to a reduced correlation coefficient and thus to significant errors. The reconstructions shown in this work will only include pixels having a correlation higher than 0.95. This was set as a criterion for using only those pixels where the correlation is strong and the matching of pixels in the images taken by the two spacecraft is thus reliable.

The size of the correlation window depends on the feature that one is trying to reconstruct. First, the window cannot be too large as we are interested in active region (AR) loops (with the width of the order of two-three pixels). If the window is too big, the spatial precision (resolution) in the estimation will be reduced. On the contrary, if the window size is too small the resulting image may be too noisy and the reconstructed features will be barely visible through the noise. We then derive the optimal window size based on the trial and error procedure. For the case of loops, the window size should be small. We use a windows size of 3×3 pixels, which is the smallest possible size, and the resulting noise levels are still acceptable. On the other hand, for large scale features the window may reach much bigger sizes (*e.g.* 100×100 pixels for a CME).

3. Results

3.1. Active Regions

We have analysed active regions (AR) detected on the solar disc from the beginning of April 2007 until the end of June 2007. We considered only the active regions reported by the NOAA Space Weather Prediction Center (they have a NOAA number). The reason for choosing this period of time relies on the fact that the separation between the two spacecraft is appropriate for reconstruction of features seen by EUVI and that there is a good number of active regions visible on the disc. We then selected the date at which each active region was closest to the center of the Sun. For that day, the least compressed image (compression ICER0) was used, *i.e.* one image pair per active region.

The first AR that we analyzed was NOAA AR 10949, as seen on 2 April 2007. We have found out that for earlier dates the angular separation (less than 3°), and thus the stereoscopic effect, is too small for our method to be used. In addition we prefer to use images taken after the commissioning period of the instruments, in order to avoid pointing errors. The last active region we analyzed is NOAA AR 10960 on 8 June 2007 (NOAA ARs 10961 and 10962 appeared close to the end of the month but did not reach central longitudes before July). For later times, the angular separation between the spacecraft becomes too big (more than 15°) and the matching of points between A and B images is more difficult and ambiguous.

Figure 1 shows the Sun as seen by SECCHI/EUVI-A on 2 May 2007, when the separation between the spacecraft was 6.2°. On this date there were two active regions clearly visible on the solar disc, NOAA AR 10953 and 10954. Figures 2, 3 and 4 show the reconstructed (3D) height above the solar surface in the 171, 195 and 284 Å passbands respectively. The observations in the three wavelengths are taken almost simultaneously. The difference in time varies depending on the date, but lies always in the range from 15 to 210 seconds. Considering that the solar rotation induces a one pixel shift (1.6″ for SECCHI/EUVI) in about 10 minutes, the difference in time between the images in the three wavelengths can be considered negligible. Neither should brightness variations in loops be affected significantly in this short period of time.

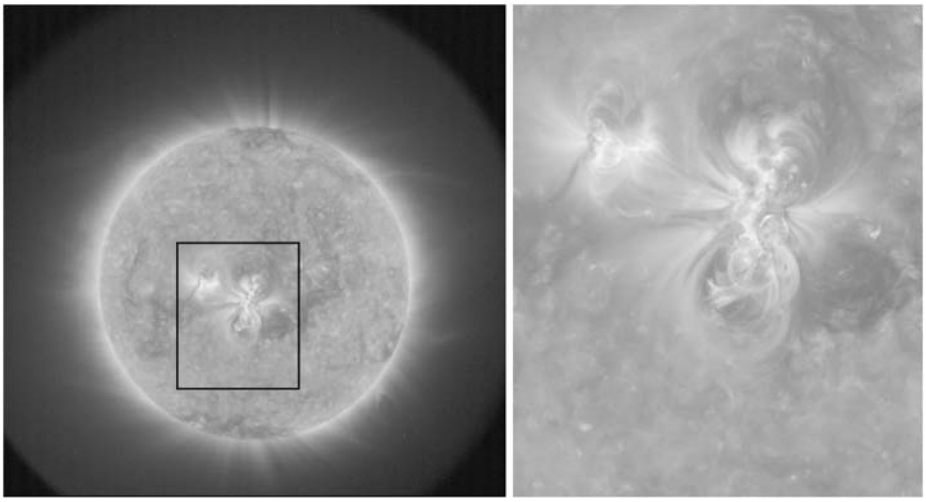

Figure 1 Left panel: SECCHI / EUVI-A image in the 171 Å bandpass taken on 2 May 2007 at 01:01:30 UT. A zoomed version of the active regions NOAA AR 10953 and 10954 (black window on left panel) stands on the right. In all the figures in this paper the north is on top and the west is to the right.

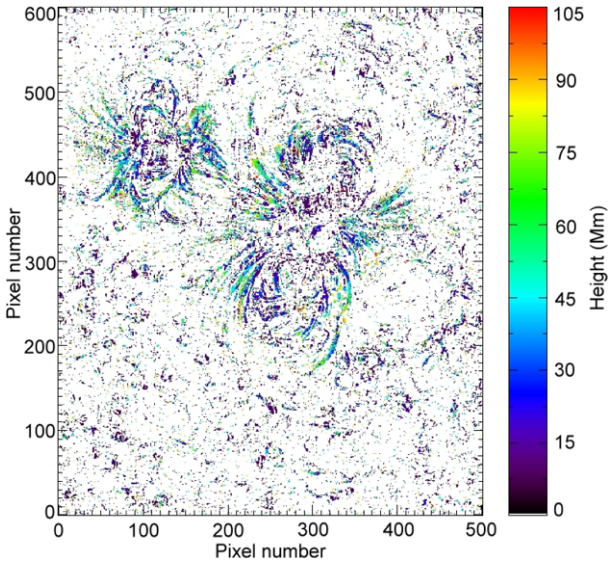

Figure 2 3D configuration of the NOAA active regions 10953 (close to the center of the image) and 10954 (in the top left corner of the image) as observed in the 171 Å bandpass, on 2 May 2007 at 01:01:30 UT. The colors show the height above the solar surface.

The loops are clearly visible in all the images as structures located above the solar surface, as one can expect. Besides loops, several bright points can be also seen (*e.g.* in the 195 Å and 284 Å bandpasses around $x = 75$, $y = 95$ in Figures 3 and 4). A significant "noise" can be seen in the quiet Sun around the active regions. Due to differences in morphology of the solar atmosphere observed in each bandpass (see *e.g.* Feldman, Widing, and Warren, 1999), there is noticeably more noise in the 171 Å bandpass. The removal of the noise is linked to a general problem of the separation of loops from the quiet Sun and is

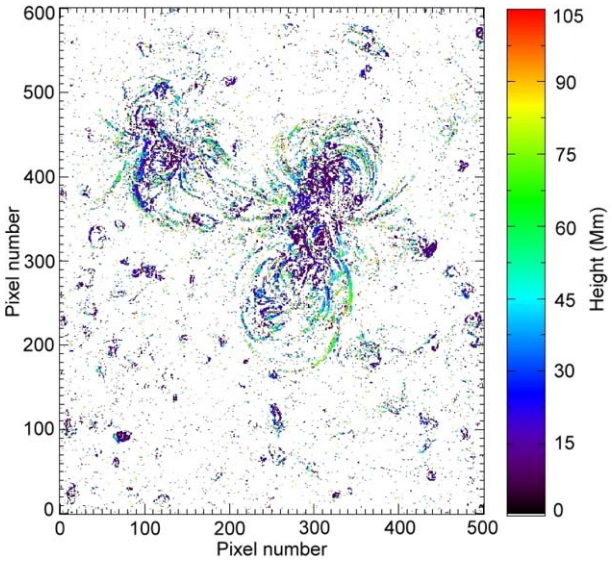

Figure 3 Same as Figure 2 but in the 195 Å passband, on 2 May 2007 at 01:02:00 UT.

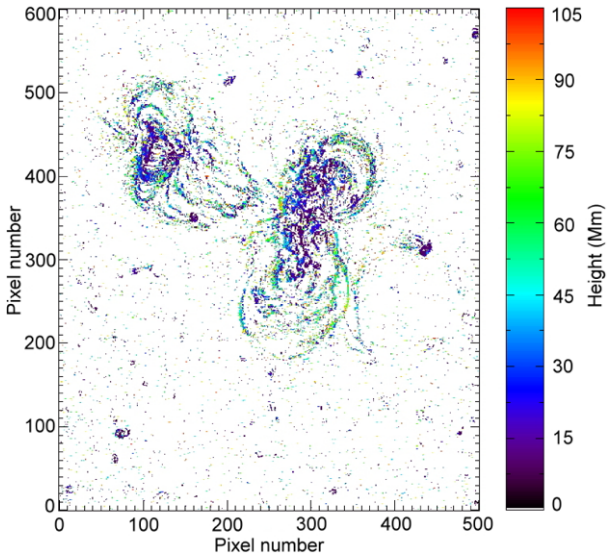

Figure 4 Same as Figure 3 but in the 284 Å passband, on 2 May 2007 at 01:00:52 UT.

out of the scope of this paper. Since we reconstruct the full image, we can simply focus on certain structures, such as loops, and not take into account the rest.

Figure 5 shows the reconstructions for the three wavelengths for NOAA active regions 10955 observed on 12 May 2007 (left panels), and 10960 observed on 8 June 2007 (right panels). On the later date (in June), the noise is clearly stronger than in May. This is a direct consequence of the increase in the angular separation between the spacecraft. As we mentioned above, large separation angles make the reconstruction using our method more difficult and prone to errors.

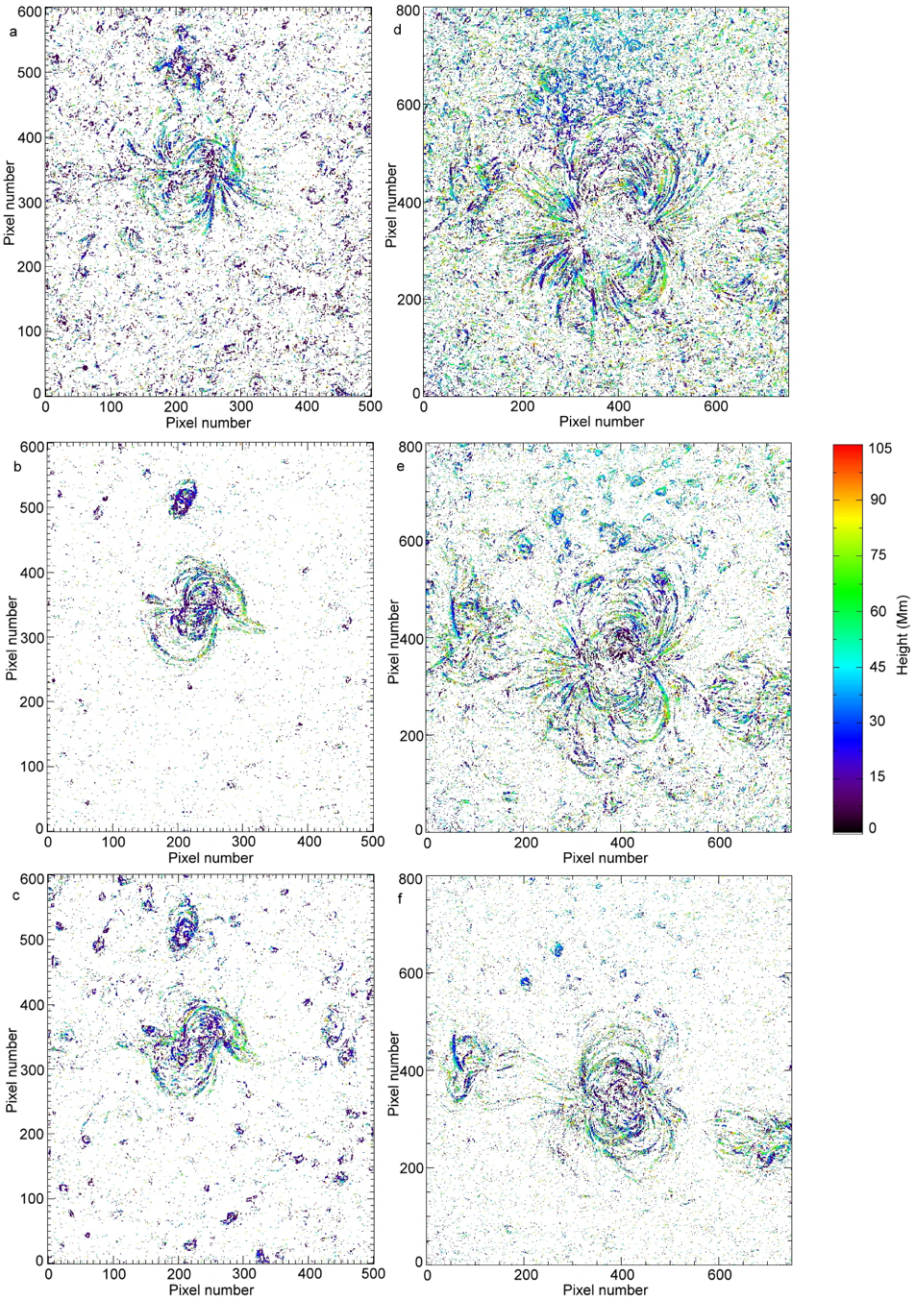

Figure 5 3D configuration of the NOAA active regions 10955 on 12 May 2007 (left panels, (a): 171 Å at 00:06:00 UT, (b): 195 Å at 00:06:15 UT, (c): 284 Å at 00:06:30 UT) and 10960 on 8 June 2007 (right panels, (d): 171 Å at 00:09:00 UT, (e): 195 Å at 00:05:30 UT, (f): 284 Å at 00:06:30 UT).

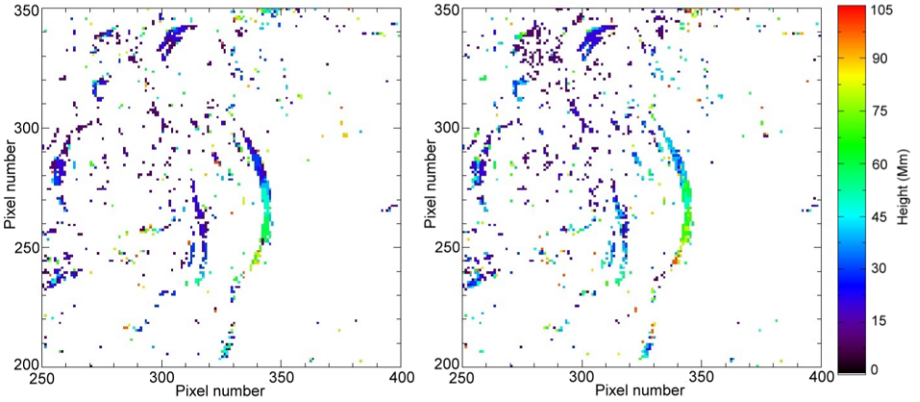

Figure 6 Left: Zoom on a segment of a loop observed in the 171 Å bandpass (pixel numbers correspond to those in Figure 2, from 2 May 2007), showing only those pixels which also have a non-zero height above the solar surface in the 195 Å image (see Figure 3). The right panel is the corresponding representation in the 195 Å passband, with only those pixels which are present above the solar surface in the 171 Å passband. The loop segment centered around (340, 270) is described in the text.

3.2. Loops

In the images taken from a single spacecraft, or even in the reconstructed maps of heights, one can easily notice several loops, or loop segments, that seem to be lying co-spatially (in the image plane) as observed simultaneously in different wavelengths. In Figure 6, we show a region containing a loop segment seen both in the 171 and 195 Å EUVI filters. These images are a zoomed part of the AR in Figure 2 (171 Å) and Figure 3 (195 Å). The values on the axes denote the region that was selected, and only the points which are present at the same location in both passbands (171 and 195 Å) are shown (*i.e.* the intersection of both images). The loop segment centered around $x = 340$ and $y = 270$ is the most prominent structure that is present in both wavelengths, at the same location. It is clearly visible that the northern portion of the loop segment (close to the footpoint) lies at lower heights than the southern portion. We can then select the pixels corresponding to this loop segment, in both wavelengths, in order to analyse their co-spatiality in three dimensions. In Figure 7 the height of each pixel for both wavelengths is displayed, with error bars considered assuming an error in the displacement of ± 1 pixel in the reconstruction formula (2). This corresponds to the error of ± 10 Mm in the reconstructed height. This error takes into account the finite resolution of the telescope in addition to a possible error in the output of the LCT method due to a lack of subpixel resolution. It is determined by the geometry of the system, where the accuracy is set by:

$$\delta h = \frac{d/2}{\tan(\Delta\lambda/2)}, \tag{3}$$

here δh represents the height accuracy, d is the pixel size and $\Delta\lambda$ is the angular separation between the two spacecraft. The value $2\delta h$ can be considered as the effective pixel size in height.

Figure 7 shows a very clear tendency of pixels seen in 195 Å to be lying higher than the corresponding 171 Å pixels, even though the error bars do intersect for many pixels. This suggests that the pixels in both wavelengths do not belong to the same loop, or at least

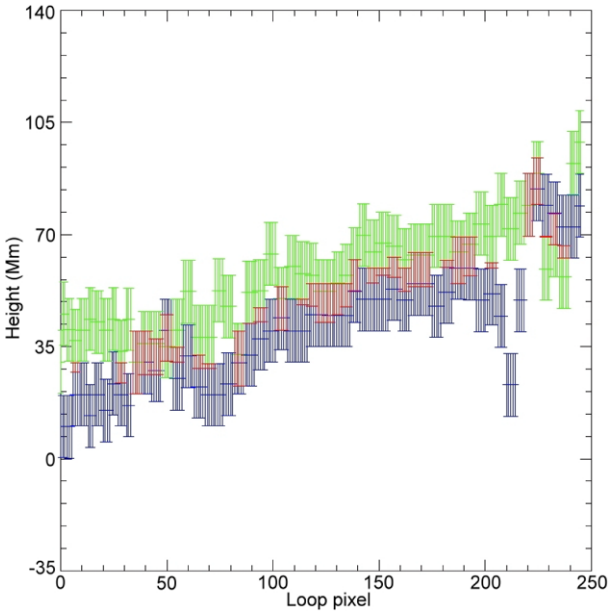

Figure 7 Height above the solar surface of the pixels corresponding to the loop segment (see Figure 6) observed in the 171 Å (blue) and the 195 Å (green) bandpasses. Red color marks the intersection of error bars for the loop heights in two passbands. Pixels are counted from the northern end of the loop segment.

not to the same portion of the loop cross-section. In Figure 8, the difference between the heights of loop pixels (the 195 Å pixel heights have been subtracted from the corresponding 171 Å pixel heights) is shown. The error bars now have double the size of the corresponding ones in Figure 7. The mean values of the height difference are located systematically below zero, confirming our hypothesis that the loops do not occupy the same volume in three-dimensional space.

If we assume that the loop emission in the 171 Å and 195 Å bandpasses comes from the same volume of plasma, then the only way to interpret our results is to conclude that our method allows us to determine the true height of a loop (the overlap between the 195 Å and 171 Å error bars shown by the red bars in Figure 7) with a very high precision. In this case, however, the height difference remains unexplained for pixels where there is no overlap between the 195 Å and 171 Å heights.

We have repeated the same analysis for a loop segment in the NOAA AR 10956 observed by STEREO on 19 May 2007 (Figure 9). The loop of interest is shown in Figure 10, after applying similar processing as the one made for Figure 6 (*i.e.* the pixels seen both in the 171 Å and 195 Å bandpasses are displayed). The loop segment under study can be found to be centered around $x = 280$, $y = 350$. Figures 11 and 12 show the pixel heights in the two bandpasses and the height difference, respectively (similar to Figures 7 and 8). Although there is a tendency for the 195 Å pixels to lie on top of the 171 Å pixels, the effect it is not so clear in this case. In particular, in the southern part of the loop the mean difference is close to zero. However, in the northern part of the loop the height difference between the pixels observed in 195 Å and 171 Å is clear. It is worth noticing that for this case, since the angular separation is higher, the (geometrical) accuracy of the determined heights is increased to ± 7 Mm.

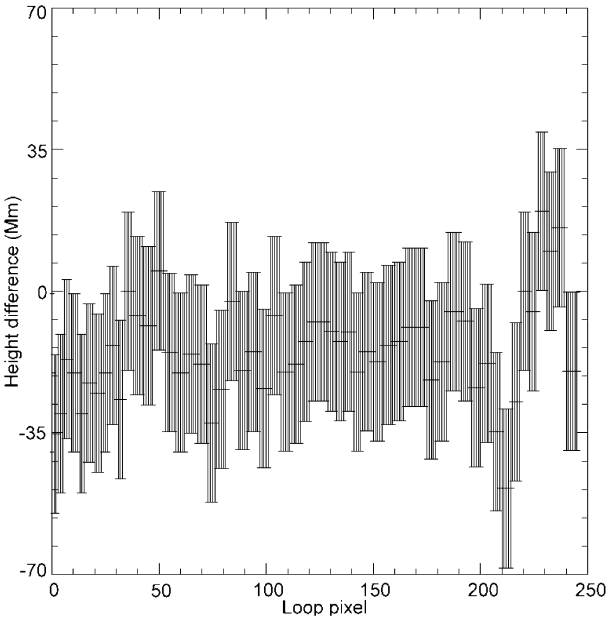

Figure 8 Difference between the heights of the two sets of points shown in Figure 6 (heights of pixels seen in the 195 Å bandpass are subtracted from heights of the same pixels seen in the 171 Å bandpass). Note that error bars have double size compared to the previous figure. Pixels are counted from the northern end of the loop segment.

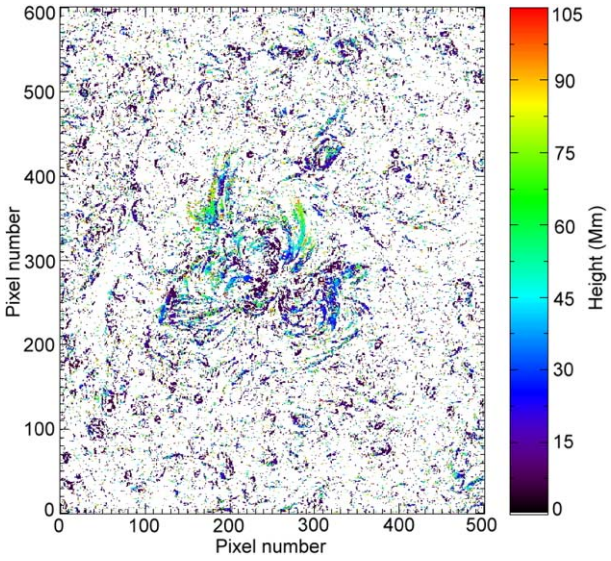

Figure 9 3D configuration of the NOAA active region 10956 as seen in the 171 Å bandpass of SECCHI/EUVI, on 19 May 2007 at 01:01:30 UT. The colors show the height above the solar surface.

4. Discussion and Conclusions

We have presented a method to obtain information on the 3D configuration of solar features using STEREO/SECCHI EUVI data. By co-aligning the images in a first step, we can then identify and match automatically the pixels in EUVI image pairs. This is done by means of a local correlation tracking technique. The output of this technique allows the straightforward calculation of 3D coordinates, taking into account the known geometry of the system (the locations of the two spacecraft). We have applied this method to reconstruct active regions

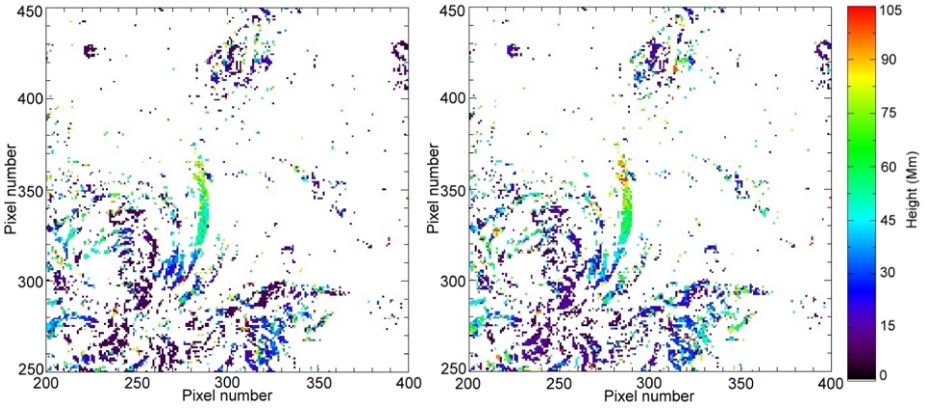

Figure 10 Left: Zoom on a loop segment observed in the 171 Å bandpass (pixel numbers correspond to those in Figure 9), showing only those pixels which are also present at the same location in the height map derived from the observations taken in the 195 Å bandpass. The right panel is the corresponding representation in the 195 Å passband, with only those pixels which have non-zero height above the solar surface in the 171 Å passband. The loop segment centered around (280, 350) is described in the text.

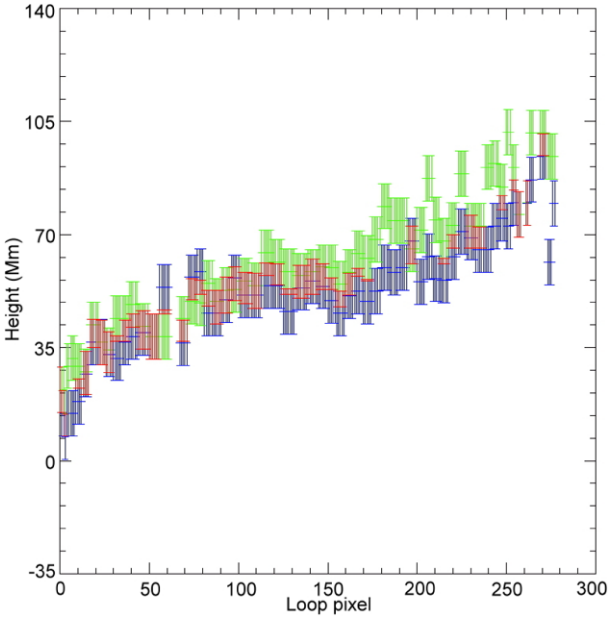

Figure 11 Height above the solar surface of the pixels corresponding to the loop segment (shown in Figure 10) observed in the 171 Å (blue) and the 195 Å (green) bandpasses. Red color marks the intersection of error bars for the loop heights in two passbands. Pixels are counted from the southern end of the loop segment.

in the 171 Å, 195 Å and 284 Å channels of EUVI. The application to the 304 Å channel (with the dominant contribution from the emission of the low transition region plasma at around 80 000 K) is by no means excluded from our technique, but it is not directly relevant for the case of active region coronal loops.

It is worth noticing that our method does not require any user interaction. Running the pixel matching and subsequent 3D reconstruction as automated processes has the advantage of eliminating any error introduced by user interaction (*e.g.* manual selection of pixels in

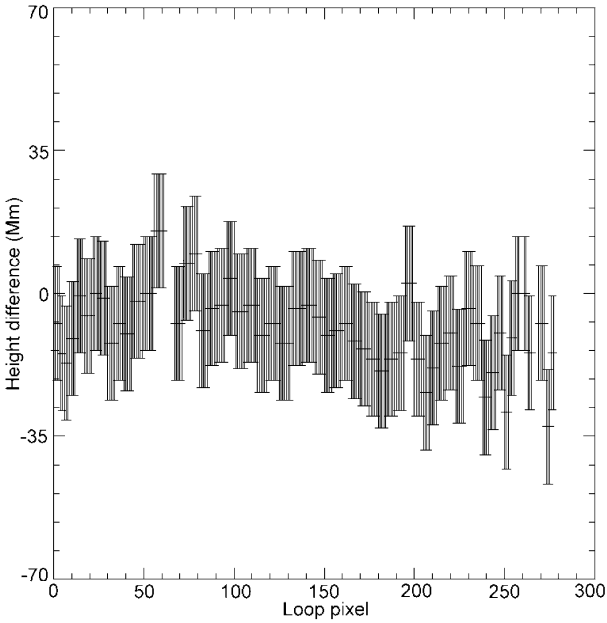

Figure 12 Difference between the two sets of points shown in Figure 10 (heights of pixels seen in the 195 Å bandpass are subtracted from heights of the same pixels seen in the 171 Å bandpass). Note that error bars have double size compared to the previous figure. Pixels are counted from the southern end of the loop segment.

the EUVI A and B images), rendering the results more objective while at the same time allowing to handle large amounts of data within a short time.

From our study of seemingly co-spatial loops (observed in different bandpasses) we have demonstrated that the emitting plasma seen to be lying co-spatially in usual images taken in projection onto the plane of the sky in more than one bandpass often do not correspond to the same plasma volume in three dimensions. There are loops which seem to be located at different heights in the corona, while still looking co-spatial in images taken by a single telescope, thus implying that the emission is not coming from the same parcel of plasma. These results should be carefully taken into account when applying filter ratio techniques to solar EUV data.

We have identified cases (*e.g.* the loop segment observed on 2 May 2007, see Figures 7 and 8) where the difference in height between the two visually co-spatial loops implies that their emission does not come from the same loop. The 195 Å loop is situated higher than its 171 Å companion. This result points towards a previously raised concern (*e.g.* Schmelz, 2002; Martens, Cirtain, and Schmelz, 2002) about calculations of loop temperature involving filter ratios. If the plasma emission sampled in the two bandpasses does not come from the same volume, as it is the case here, then filter ratio techniques cannot be applied meaningfully. It is important to stress that our result is deduced from two-viewpoint measurements and is thus an independent confirmation of previous results (*e.g.* Schmelz, 2002; Martens, Cirtain, and Schmelz, 2002).

In Figure 8, the average difference between loop heights is -15 Mm and the standard deviation amounts to 11 Mm. Therefore, even considering the pixel-to-pixel variation in the values, the 195 Å loop is on top of its 171 Å companion. The average value of the height difference (15 Mm) is several times larger than the observed loop width (2 – 4 pixels, *i.e.* around 2 – 4 Mm). This means that, assuming a circular loop cross-section, the height difference between the 171 Å and 195 Å loops is statistically significant. However, the accuracy of the height reconstruction is rather low (the effective pixel size in height is 20 Mm). This

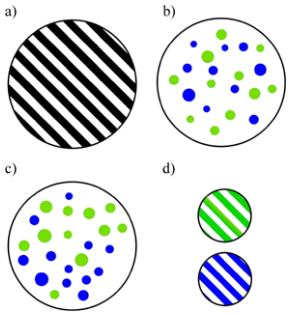

Figure 13 Four different possibilities for the results obtained (see text): (a) Isothermal loop emitting both in 171 Å and 195 Å. (b) Loop consisting of nearly isothermal strands emitting in 195 Å (green circles) and 171 Å (blue circles). (c) Same as (b), but the strands are now distributed in such a way that the hotter ones (195 Å, green circles) are on average situated higher than the 171 Å ones (blue circles). (d) Two different loops emitting in 195 Å (green) and 171 Å (blue).

is shown by overlapping error bars for many pixels in Figure 7. It is thus still possible (although less likely) that we are looking at the same loop emitting in both 171 Å and 195 Å bandpasses. For the loop height differences shown in Figure 12, the average value is -8 Mm and the standard deviation is 8 Mm. In this case it is not so clear that one loop is higher than the other one as the error bars of the height difference are rather large (± 14 Mm).

When dealing with EUV observations of the solar corona, one can never discard the influence of the integration of optically thin plasma emission along the line of sight. The overlap of our error bars can also be a consequence of this effect if one recalls that the temperature response curves for the 195 Å and 171 Å passbands overlap (see Figure 7 in the paper by Howard *et al.*, 2008). The peaks of both temperature response curves lie close to the peak of the differential emission measure (DEM) distribution for active regions, which is generally situated between 1 MK and 1.5 MK (*e.g.* Brosius *et al.*, 1996; Landi and Feldman, 2008). It is possible that our results reflect the height distribution of unresolved isothermal loop strands emitting at different temperatures near the DEM peak. Indeed, an insufficient spatial resolution to resolve single loops might be added to the list of possible reasons for the overlapping (but not coinciding) loop pixel height ranges shown by error bars in Figures 7 and 11. In fact, the effective spatial resolution of EUVI was estimated to be 2 pixels by Wuelser *et al.* (2004), which translates to 2.3 Mm. Aschwanden and Nightingale (2005) studied 2512 TRACE loops and found a mean loop width of 1.42 Mm. By considering a circular cross-section for the loops, this width would be the same in the vertical direction. Our results may then indicate that the reconstructed features are comprised of several unresolved narrower loop strands, perhaps emitting in both 171 Å and 195 Å wavelengths. If this were the case, the loop strands emitting mostly in the 195 Å and mostly in the 171 Å would be mixed inside the same volume, but with the 195 Å loops lying on average higher than the 171 Å loops. The different possibilities outlined here are depicted in Figure 13. Our results can thus be interpreted in terms of the third option (c) shown in the cartoons. The option shown in Figure 13(d) is not excluded either, but the geometrical accuracy of the stereoscopic reconstruction makes it difficult to differentiate between these two options.

A possible physical mechanism responsible for the difference in height between cooler and hotter loops or loop strands (emitting mostly in 171 Å and 195 Å bandpasses respectively) may be linked to the hydrostatic scaling. As the hydrostatic scale height $H \sim \frac{kT}{m_{\rm p}g}$ is proportional to the temperature T (k is the Boltzmann constant, $m_{\rm p}$ is the proton mass and g is the solar gravitational acceleration), we expect hotter plasma to be dominantly higher

in the corona, with density determined as $n = n_0 \exp(-\frac{h}{H})$ (n_0 is footpoint density and h is height above the solar surface). The height difference between two loop strands with different temperatures can then be explained as follows. Due to the low plasma beta ($\beta \sim \frac{nkT}{B^2/8\pi}$, the ratio between the thermal and magnetic pressure) in active region loops, the plasma is constrained by the magnetic field lines. Other forces, including the gradient of thermal pressure $p \sim nkT$, are small in comparison with the magnetic forces, but they slightly modify the position of the mechanical equilibrium for loop strands. Due to the hydrostatic scaling, the plasma density at the loop top should be higher in a hotter loop strand (assuming equal footpoint density n_0 for both strands). The plasma pressure gradient force $-\nabla p \sim m_{\rm p} g n$ at the loop top would be thus higher in the hotter loop strand (although still small compared to the magnetic forces). As the plasma pressure gradient force is directed upwards, it will provide a small height difference between two strands. It is thus possible that of two nearby strands (Figure 13(c)) with nearly identical magnetic field configuration, the hotter strand is located slightly higher than the cooler strand. Other explanations may exist, but a detailed investigation of this issue is out of scope of the present paper.

Apart from active regions and loops, our method can be applied to various types of studies which have not been described here. For example the EUVI data taken in the 304 Å bandpass allow us to calculate filaments' heights (see *e.g.* Gissot *et al.*, 2008). Structures seen off-limb (loops, filaments, polar plumes, etc) can be unambiguously traced in order to determine if they are lying ahead or behind the plane of the sky, which is very important for example, in CME studies.

Acknowledgements We thank the STEREO-SECCHI team for the use of EUVI data. We acknowledge support from the Belgian Federal Science Policy Office through the ESA-PRODEX programme. The authors wish to thank Bernd Inhester for fruitful discussions.

References

Aschwanden, M.J., Bastian, T.S.: 1994, *Astrophys. J.* **426**, 425.
Aschwanden, M.J., Nightingale, R.W.: 2005, *Astrophys. J.* **633**, 499.
Aschwanden, M.J., Lim, J., Gary, D.E., Klimchuk, J.A.: 1995, *Astrophys. J.* **454**, 512.
Aschwanden, M.J., Newmark, J.S., Delaboudinière, J.-P., Neupert, W.M., Klimchuk, J.A., Gary, G.A., *et al.*: 1999, *Astrophys. J.* **515**, 842.
Aschwanden, M.J., Wuelser, J.-P., Nitta, N.V., Lemen, J.R.: 2008, *Astrophys. J.* **679**, 827.
Alexander, D., Katsev, S.: 1996, *Solar Phys.* **167**, 153.
Berton, R., Sakurai, T.: 1985, *Solar Phys.* **96**, 93.
Brosius, J.W., Davila, J.M., Thomas, R.J., Monsignori Fossi, B.C.: 1996, *Astrophys. J. Suppl.* **106**, 143.
Dymova, M.V., Ruderman, M.S.: 2006, *Astron. Astrophys.* **459**, 241.
Feldman, U., Widing, K.G., Warren, H.P.: 1999, *Astrophys. J.* **522**, 1133.
Feng, L., Wiegelmann, T., Inhester, B., Solanki, S., Gan, W.Q., Ruan, P.: 2007a, *Solar Phys.* **241**, 235.
Feng, L., Inhester, B., Solanki, S.K., Wiegelmann, T., Podlipnik, B., Howard, R.A., Wuelser, J.-P.: 2007b, *Astrophys. J.* **671**, L205.
Gissot, S.F., Hochedez, J.-F., Chainais, P., Antoine, J.-P.: 2008, *Solar Phys.* **252**, 397.
Howard, R.A., Moses, J.D., Vourlidas, A., Newmark, J.S., Socker, D.G., Plunkett, S.P., *et al.*: 2008, *Space Sci. Rev.* **136**, 67.
Inhester, B.: 2006, *Publ. Int. Space Sci. Inst.* astro-ph/0612649.
Kaiser, M.L., Kucera, T.A., Davila, J.M., St. Cyr, O.C., Guhathakurta, M., Christian, E.: 2008, *Space Sci. Rev.* **136**, 5.
Kouchmy, S., Molodensky, M.M.: 1992, *Nature* **360**, 717.
Landi, E., Feldman, U.: 2008, *Astrophys. J.* **672**, 674.
Martens, P.C.H., Cirtain, J.W., Schmelz, J.T.: 2002, *Astrophys. J.* **577**, L115.
Mierla, M., Davila, J., Thompson, W., Inhester, B., Srivastava, N., Kramar, M., *et al.*: 2008, *Solar Phys.* **252**, 385.
November, L.J., Simon, G.W.: 1988, *Astrophys. J.* **333**, 427.

Patsourakos, S., Pariat, E., Vourlidas, A., Antiochos, S.K., Wuelser, J.P.: 2008, *Astrophys. J.* **680**, L73.
Trucco, E., Verri, A.: 1998, *Introductory Techniques for 3-D Computer Vision*, Prentice Hall, New York.
Schmelz, J.T.: 2002, *Astrophys. J.* **578**, L161.
Wuelser, J.-P., Lemen, J.R., Tarbell, T.D., Wolfson, C.J., Cannon, J.C., Carpenter, B.A., *et al.*: 2004, In: Fineschi, S., Gummin, M.A. (eds.) *Telescopes and Instrumentation for Solar Astrophysics*, *Proceedings of the SPIE* **5171**, 111.